TU Delft

Delft University of Technology

Deconvolution of azimuthal mode detection measurements

Sijtsma, Pieter; Brouwer, Harry

DOI
10.1016/j.jsv.2018.02.029

Publication date
2018

Document Version
Accepted author manuscript

Published in
Journal of Sound and Vibration

Citation (APA)
Sijtsma, P., & Brouwer, H. (2018). Deconvolution of azimuthal mode detection measurements. *Journal of Sound and Vibration*, *422*, 1-14. https://doi.org/10.1016/j.jsv.2018.02.029

Important note
To cite this publication, please use the final published version (if applicable).
Please check the document version above.

Copyright
Other than for strictly personal use, it is not permitted to download, forward or distribute the text or part of it, without the consent of the author(s) and/or copyright holder(s), unless the work is under an open content license such as Creative Commons.

Takedown policy
Please contact us and provide details if you believe this document breaches copyrights.
We will remove access to the work immediately and investigate your claim.

This work is downloaded from Delft University of Technology.
For technical reasons the number of authors shown on this cover page is limited to a maximum of 10.

Deconvolution of Azimuthal Mode Detection Measurements

Pieter Sijtsma[1,2,*], Harry Brouwer[3]

1 PSA3, Prinses Margrietlaan 13, 8091 AV Wezep, The Netherlands
2 Aircraft Noise & Climate Effects, Faculty of Aerospace Engineering, Delft University of Technology, P.O. Box 5058, 2600 GB Delft, The Netherlands
3 Department of Helicopters & Aeroacoustics, Netherlands Aerospace Centre NLR, P.O. Box 90502, 1059 CM Amsterdam, The Netherlands
*Corresponding author: Pieter.Sijtsma@psa3.nl

Abstract

Unequally spaced transducer rings make it possible to extend the range of detectable azimuthal modes. The disadvantage is that the response of the mode detection algorithm to a single mode is distributed over all detectable modes, similarly to the Point Spread Function of Conventional Beamforming with microphone arrays. With multiple modes the response patterns interfere, leading to a relatively high "noise floor" of spurious modes in the detected mode spectrum, in other words, to a low dynamic range. In this paper a deconvolution strategy is proposed for increasing this dynamic range. It starts with separating the measured sound into shaft tones and broadband noise. For broadband noise modes, a standard Non-Negative Least Squares solver appeared to be a perfect deconvolution tool. For shaft tones a Matching Pursuit approach is proposed, taking advantage of the sparsity of dominant modes. The deconvolution methods were applied to mode detection measurements in a fan rig. An increase in dynamic range of typically 10 to 15 dB was found.

Nomenclature

$\mathbf{a}$	CB amplitude vector
a_k	CB amplitude
$\mathbf{A}$	CB Mode Cross-Spectral Matrix
$\mathbf{b}$	mode amplitude vector
b_k	mode amplitude
$\mathbf{B}$	Mode Cross-Spectral Matrix
$\mathbf{C}$	Cross-Spectral Matrix

$\mathbf{g}$, $\mathbf{g}_k$	steering vector
g_n, $g_{k,n}$	steering vector element
$\mathbf{G}$	steering matrix
i	imaginary unit
j	azimuthal mode order
J	cost function
k	azimuthal mode order
K	number of modes
n	transducer index
N	number of transducers
$\mathbf{p}$	pressure vector
p_n	pressure amplitudes
$\mathbf{Q}$	convolution matrix
Q_{kj}	Point Spread Function
$\mathbf{S}$	convolution matrix for incoherent modes
S_{kj}	elements of $\mathbf{S}$
u_k	CB mode auto-power
$\mathbf{U}$	CB mode auto-power vector
v_k	mode auto-power
$\mathbf{V}$	mode auto-power vector
$\mathbf{w}_k$	weight vector
$\mathbf{W}$	weight matrix
Π_k	Point Spread Function
$(.)_{\mathrm{brb}}$	broadband (non-periodic)
$(.)_{\mathrm{dec}}$	deconvolved
$(.)_{\mathrm{res}}$	residual
$(.)_{\mathrm{sub}}$	subset of detectable modes
$(.)_{\mathrm{ton}}$	tonal (shaft-periodic)
BPF	Blade Passing Frequency
CB	Conventional Beamforming
CSM	Cross-Spectral Matrix
DFT	Direct Fourier Transform
MCSM	Mode Cross-Spectral Matrix
MP	Matching Pursuit
NNLS	Non-Negative Least Squares
PSF	Point Spread Function
SPL	Sound Pressure Level

1. Introduction

Decomposition of the acoustic field into its azimuthal components can reveal valuable information about sound generating mechanisms. For that reason so-called “mode detection measurements”, aiming at performing such decompositions, are standard tools in experimental engine noise studies with fan rigs [1], static full-size engine tests [2], and flight measurements [3]. The distribution of azimuthal (or circumferential or spinning) modes of shaft order tones provides insight in phenomena like rotor-stator interaction noise [4], steady flow distortion noise [5] and scattering by liner splices [3]. Modal information of broadband noise is useful too, for example in combination with phased array beamforming [6].

Azimuthal mode measurements are typically performed with ring-shaped arrays of microphones (or pressure transducers). Such arrays don’t provide information about radial modes. These can be measured by means of radial rakes instrumented with pressure transducers [7-10] or by means of a rotating axial transducer array mounted flush in the duct wall [8].

The most natural array for mode detection is a ring of equally spaced transducers. Then the inversion problem that needs to be solved to obtain, at a given frequency, the amplitudes of the modes features an orthogonal matrix, which is easily inverted. The resulting modal amplitudes can be evaluated with a Direct Fourier Transform (DFT) applied to the transducer pressure amplitudes. The number of modes that can be detected is equal to the number of transducers. The Nyquist-Shannon sampling criterion implies that the absolute mode order should be less than half the number of transducers. Aliasing occurs when higher order modes exist.

The range of modes that can be measured without aliasing can be extended by using a non-equally spaced array [1]. But then the inversion problem and the DFT solution are no longer equivalent. The inversion problem cannot deal with more modes than transducers, and the DFT method introduces the detection of spurious modes [1].

When the analysis is restricted to tonal (shaft-periodic) sound, advantage can be taken from the fact that the sound field is usually dominated by a limited set of modes. This “sparsity” of modes has recently [11,12] been exploited by applying Compressed (or Compressive) Sensing, which is a signal processing technique aiming at representing measured data with fewer samples than prescribed by the Nyquist-Shannon sampling criterion. The Compressed Sensing technique features the minimisation of the L1-norm of the vector of mode amplitudes. By application of an extended version of the Orthogonal Matching Pursuit algorithm a maximum number of dominant modes is determined accurately with a given array and after a deconvolution step the remaining mode spectrum is estimated using e.g. the DFT [11]. For broadband noise, of which the acoustic energy is more equally distributed over the mode orders, this may not be the most appropriate approach.

This paper proposes a strategy based on deconvolution, using lessons learned from methods that were developed over the past decade for microphone array measurements [13-19], and exploiting the fact that

the DFT method for azimuthal mode detection is exactly the same as Conventional Beamforming (CB) with microphone arrays [20]. Deconvolution methods start with CB and aim at retrieving source amplitudes using the known CB response of individual sources. In this paper, broadband noise and tonal sound are considered separately. Deconvolution of broadband noise is done with a Non-Negative Least Squares (NNLS) solver, similar to DAMAS [14]. For tonal sound a Matching Pursuit algorithm is used, similar to the approach followed in a few phased array deconvolution methods before [19,21].

The next chapter gives a mathematical description of the proposed deconvolution strategy. In Chapter 3 mode detection deconvolution is applied to fan rig measurements. Chapter 4 gives a brief discussion about the quality of the deconvolution data, followed by the conclusions in Chapter 5.

2. Mathematical description

All methods and results discussed in this paper are applied to single frequencies or frequency bins. For brevity, the frequency-dependence is omitted in the mathematical expressions. Measured (complex) pressure amplitudes must be understood as the results of Fourier transforms applied to the time data. The terminology of acoustic beamforming is used.

2.1. Beamforming basics

2.1.1. Steering vector

Beamforming starts with the definition of a steering function to describe the response from a potential target to a microphone. Usually, the target is a point source position and the steering function is a Green's function solution of the Helmholtz equation. A steering vector **g** consists of the steering function values of a fixed target, evaluated at *N* microphone locations.

Azimuthal mode detection can also be treated like beamforming, considering the mode orders as targets. The steering function is then $\exp(-\mathrm{i}k\theta)$, where θ is the microphone's angular position and k the mode order k, describing the azimuthal periodicity. Thus, for the steering vector elements, we have

$$g_n = \exp(-\mathrm{i}k\theta_n), \tag{1}$$

where θ_n is the angular position of the n-th transducer.

Given a pressure vector **p** (vector of measured pressure amplitudes p_n) and a set of K steering vectors $\mathbf{g}_k$, the model assumption is that a set of mode amplitudes b_k exists such that

$$\mathbf{p} = \sum_k b_k \mathbf{g}_k \,, \tag{2}$$

with

$$g_{k,n} = \exp(-\mathrm{i}k\theta_n). \tag{3}$$

We can write the source model equation, Eq. (2), in condensed form:

$$\mathbf{p} = \mathbf{G}\mathbf{b}, \tag{4}$$

where **b** is the *K*-dimensional "mode amplitude vector" and **G** the *N*×*K*-dimensional "steering matrix", the columns of which are the steering vectors.

2.1.2. Conventional Beamforming

The Conventional Beamforming (CB) approach to find approximate source amplitudes a_k is to determine, for each unknown mode order separately, a best match with the measured data by minimizing:

$$J = \left\| \mathbf{p} - a_k \mathbf{g}_k \right\|^2 . \tag{5}$$

The minimum value of the cost function *J* is found for

$$a_k = \mathbf{w}_k^* \mathbf{p} , \tag{6}$$

where the asterisk stands for "complex conjugate transpose" and the "weight vector" $\mathbf{w}_k$ is given by

$$\mathbf{w}_k = \frac{1}{\mathbf{g}_k^* \mathbf{g}_k} \mathbf{g}_k . \tag{7}$$

Evaluating Eq. (6) with Eq. (3) yields

$$a_k = \frac{1}{N} \sum_{n=1}^{N} p_n \exp\left(\mathrm{i} k \theta_n\right), \tag{8}$$

which is identical to the DFT expression used by Rademaker et al. [1].

The CB expression, Eq. (6), can be written in condensed form too:

$$\mathbf{a} = \mathbf{W}^* \mathbf{p} , \tag{9}$$

where **W** is the *N*×*K*-dimensional "weight matrix" and **a** the *K*-dimensional "CB amplitude vector".

2.1.3. Convolution

By combining the source model equation, Eq. (4), and the CB expression, Eq. (9), we obtain

$$\mathbf{a} = \mathbf{Q}\mathbf{b} , \tag{10}$$

in which the *K*×*K*-dimensional convolution matrix **Q** is defined by

$$\mathbf{Q} = \mathbf{W}^* \mathbf{G} . \tag{11}$$

The challenge of deconvolution methods is to solve **b** from Eq. (10).

For equally-spaced mode detection arrays it can be shown that **Q** is the identity matrix, which means that CB yields the correct mode amplitudes. Otherwise, Eq. (10) describes convolution, which is the linear combination of responses of single unit modes $\mathbf{b} = \mathbf{e}_j$. For the response of a unit mode order *j* to mode order *k* we have

$$a_k = \left(\mathbf{Q}\mathbf{e}_j\right)_k = Q_{kj} = \mathbf{w}_k^* \mathbf{g}_j . \tag{12}$$

This is the so-called Point Spread Function (PSF). Evaluating Q_{kj} with Eq. (3) yields

$$Q_{kj} = \frac{1}{N} \sum_{n=1}^{N} \exp\left[\mathrm{i}\left(k - j\right)\theta_n\right] \stackrel{\text{def}}{=} \Pi_{k-j} . \tag{13}$$

In general, the rank of the matrix **Q** is smaller than its dimension and it cannot be inverted.

2.1.4. Ensemble averaging

Estimates of the mode cross-spectral data can be obtained by multiplying the amplitude vector **b** with its conjugate transpose, and averaging the results over many time blocks. With Eq. (9) the following estimate of the Mode Cross-Spectral Matrix (MCSM) is obtained:

$$\mathbf{A} = \left\langle \mathbf{a}\mathbf{a}^* \right\rangle = \mathbf{W}^* \left\langle \mathbf{p}\mathbf{p}^* \right\rangle \mathbf{W} = \mathbf{W}^* \mathbf{C} \mathbf{W}, \tag{14}$$

where **C** is the traditional Cross-Spectral Matrix (CSM). With Eq. (4) we obtain the following convolution expression:

$$\mathbf{A} = \mathbf{W}^* \mathbf{G} \left\langle \mathbf{b}\mathbf{b}^* \right\rangle \mathbf{G}^* \mathbf{W} = \mathbf{Q} \left\langle \mathbf{b}\mathbf{b}^* \right\rangle \mathbf{Q}^* = \mathbf{Q}\mathbf{B}\mathbf{Q}^*, \tag{15}$$

where **B** is the actual MCSM. Eq. (15) is an order of magnitude more difficult to solve than Eq. (10), unless simplifying assumptions can be made for **B**. These will be discussed in the following section.

2.2. Tonal sound and broadband noise

Sound in an engine duct can typically be split into a part that is periodic with the shaft rotation and a non-periodic part. The periodic sound is a set of "shaft order" tones (i.e., the frequencies are multiples of the shaft rotation frequency), and is therefore referred to as "tonal". The frequency spectrum can be obtained by performing "phase locked" Fourier transforms [1] and averaging over many shaft revolutions:

$$\mathbf{p}_{\text{ton}} = \left\langle \mathbf{p} \right\rangle. \tag{16}$$

The remaining non-periodic sound is called "broadband noise":

$$\mathbf{p}_{\text{brb}} = \mathbf{p} - \mathbf{p}_{\text{ton}}. \tag{17}$$

Averaging over many shaft revolutions yields for the CSM:

$$\mathbf{C} = \left\langle \mathbf{p}\mathbf{p}^* \right\rangle = \mathbf{p}_{\text{ton}}\mathbf{p}_{\text{ton}}^* + \left\langle \mathbf{p}_{\text{brb}}\mathbf{p}_{\text{brb}}^* \right\rangle = \mathbf{p}_{\text{ton}}\mathbf{p}_{\text{ton}}^* + \mathbf{C}_{\text{brb}}. \tag{18}$$

Likewise, for the MCSM we have

$$\mathbf{B} = \mathbf{b}_{\text{ton}}\mathbf{b}_{\text{ton}}^* + \mathbf{B}_{\text{brb}}. \tag{19}$$

By inserting Eq. (18) into Eq. (14) we find for the estimated MCSM

$$\mathbf{A} = \left(\mathbf{W}^*\mathbf{p}_{\text{ton}}\right)\left(\mathbf{W}^*\mathbf{p}_{\text{ton}}\right)^* + \mathbf{W}^*\mathbf{C}_{\text{brb}}\mathbf{W}. \tag{20}$$

Thus, we can split the convolution into a tonal part:

$$\mathbf{A}_{\text{ton}} = \left(\mathbf{W}^*\mathbf{p}_{\text{ton}}\right)\left(\mathbf{W}^*\mathbf{p}_{\text{ton}}\right)^* = \left(\mathbf{Q}\mathbf{b}_{\text{ton}}\right)\left(\mathbf{Q}\mathbf{b}_{\text{ton}}\right)^* \tag{21}$$

and a broadband part

$$\mathbf{A}_{\text{brb}} = \mathbf{W}^*\mathbf{C}_{\text{brb}}\mathbf{W} = \mathbf{Q}\mathbf{B}_{\text{brb}}\mathbf{Q}^*. \tag{22}$$

The tonal part of the convolution is equivalent to

$$\mathbf{a}_{\text{ton}} = \mathbf{W}^{*}\mathbf{p}_{\text{ton}} = \mathbf{Q}\mathbf{b}_{\text{ton}} . \tag{23}$$

2.3. Deconvolution of broadband noise modes

The starting point is $\mathbf{A} = \mathbf{A}_{\text{brb}}$, obtained by evaluating the first equality of Eq. (22), and the challenge is to obtain a better estimate for $\mathbf{B} = \mathbf{B}_{\text{brb}}$ using the convolution expression

$$\mathbf{A} = \mathbf{Q}\mathbf{B}\mathbf{Q}^{*} . \tag{24}$$

For broadband noise in an engine duct it's reasonable to assume that modes with different orders are incoherent (see Appendix A). This means that the off-diagonal terms in **A** and **B** can be set to zero, leading to

$$\text{diag}(\mathbf{U}) = \mathbf{Q}\,\text{diag}(\mathbf{V})\mathbf{Q}^{*} , \tag{25}$$

where **V** is the vector of actual mode auto-powers, $v_k = B_{kk}$, and **U** the vector of CB-estimated mode auto-powers, $u_k = A_{kk}$. We can derive:

$$\mathbf{U} = \mathbf{S}\mathbf{V} , \tag{26}$$

where the $K \times K$-dimensional matrix **S** is defined by

$$S_{kj} = \left| Q_{kj} \right|^2 . \tag{27}$$

When solving Eq. (26), the constraint of non-negativity needs to be put on the elements of **V**, being auto-powers.

The problem of finding non-negative solutions of Eq. (26) is a key issue in microphone array deconvolution methods, when the assumption of incoherent sources is made. A well-known algorithm to solve the problem is DAMAS, proposed by Brooks and Humphreys [14], which features a Gauss-Seidel procedure where negative solutions are replaced by zero. Faster solution strategies were proposed by Dougherty et al., through the assumption of PSF shift-invariance [13] or by using Linear Programming [18].

For azimuthal mode detection, when the number of unknown sources is much smaller than a typical number of scan points used with beamforming, the standard Non-Negative Least Squares algorithm proposed by Lawson and Hanson [22] can be used[1]. This solver, which we denote by "NNLS", is a so-called "active set" method, in which negative solutions for v_k are set to zero, similarly to DAMAS. This is a useful trick to make the solution space sparser when the number of possible modes is larger than the rank of **S**. The advantage of NNLS is that it always comes to an end after a finite number of iterations, whereas DAMAS doesn't have a clear stop criterion.

2.4. Deconvolution of tonal modes

The starting point is now $\mathbf{a} = \mathbf{a}_{\text{ton}}$, obtained with the first equality of Eq. (23), and the challenge is obtain a better estimate for $\mathbf{b} = \mathbf{b}_{\text{ton}}$ using the convolution expression

[1] The Matlab implementation of the Lawson-Hanson NNLS algorithm is "lsqnonneg".

$$\mathbf{a} = \mathbf{Q}\mathbf{b} \,. \tag{28}$$

By definition, Eq. (11), the rank of **Q** is at most max{*K*,*N*}. Thus, if the number *K* of detectable modes is larger than the number *N* of transducers, Eq. (28) is not invertible. The NNLS trick of replacing negative results by zero doesn't work either, as there is not a non-negativity constraint. Unlike Eq. (26), which is a real-valued system, Eq. (28) is complex-valued. In this case, a Matching Pursuit (MP) algorithm, as used in a few phased array deconvolution methods before [19,21], can improve the results. The idea is to find a "best match" for Eq. (28) with a limited set of modes, as detailed below.

From the set of detectable modes, a subset of K_{sub} modes is considered with the largest absolute values of b_k. Typically, K_{sub} is much less than *N*. Assuming that this set is known, we can estimate the corresponding amplitudes b_k by minimizing

$$J = \left\| \mathbf{a} - \mathbf{Q}_{\text{sub}} \mathbf{b}_{\text{sub}} \right\|^2 . \tag{29}$$

Herein, $\mathbf{b}_{\text{sub}}$ is a K_{sub}-dimensional vector with only the subset amplitudes, and $\mathbf{Q}_{\text{sub}}$ is a $K \times K_{\text{sub}}$-dimensional matrix containing only the subset PSFs. The solution that minimises Eq. (29) is the Moore-Penrose pseudoinverse:

$$\mathbf{b}_{\text{sub}} = \left(\mathbf{Q}_{\text{sub}}^* \mathbf{Q}_{\text{sub}} \right)^{-1} \mathbf{Q}_{\text{sub}}^* \mathbf{a} \,. \tag{30}$$

Defining a "residual" CB amplitude vector by

$$\mathbf{a}_{\text{res}} = \mathbf{a} - \mathbf{Q}_{\text{sub}} \mathbf{b}_{\text{sub}} \,, \tag{31}$$

the deconvolved amplitude vector is given by

$$\mathbf{a}_{\text{dec}} = \mathbf{b}_{\text{sub}} + \mathbf{a}_{\text{res}} \,. \tag{32}$$

The effects of convolution are then only present in the residual mode amplitudes in the $\mathbf{a}_{\text{res}}$ vector.

The question remains how to find the subset containing the dominant modes. This can be done by the following iteration strategy in which a fixed (chosen) subset dimension, K_{sub}, is used:

Step 0. Determine **a** by CB, set $\mathbf{a}_{\text{dec}} = \mathbf{a}$ and start with an empty mode subset.

Step 1. Define a new mode subset by the K_{sub} largest absolute values of $\mathbf{a}_{\text{dec}}$. When the new subset is the same as the old subset, stop the iteration.

Step 2. Calculate $\mathbf{b}_{\text{sub}}$ from Eq. (30).

Step 3. Calculate $\mathbf{a}_{\text{res}}$ from Eq. (31).

Step 4. Calculate $\mathbf{a}_{\text{dec}}$ from Eq. (32).

Step 5. Return to Step 1.

The iteration is terminated when the mode subset doesn't change anymore, and the solution remains the same. This happens after a finite number of iterations, typically less than 10. The choice of the number of subset modes, K_{sub}, can be informed by looking at the condition numbers of the matrices $\mathbf{Q}_{\text{sub}}^* \mathbf{Q}_{\text{sub}}$. These condition numbers increase with K_{sub}, but should not be too large.

The Matching Pursuit approach outlined above, featuring a fixed K_{sub}, is different from the standard "Greedy Algorithm", which starts with $K_{\text{sub}}=1$ and adds a solution at each iteration step. The procedure followed here needs less iterations and is thus faster.

3. Application to fan rig mode detection data

The deconvolution techniques described in the previous chapter were applied to measurements performed in the AneCom AeroTest facility on a Rolls-Royce fan rig. Fig. 1 shows a drawing of the rig. The internal diameter was approximately 80 cm. Two mode detection arrays were installed. The first one consisted of 100 Endevco transducers, mounted in the outer surface of the bypass duct, approximately 15 cm downstream of the 44-vaned stator. The second array consisted of 100 Kulite transducers, mounted in the (drooped) intake, about 40 cm ahead of the 20-blades rotor. A liner was installed between the rotor and the array.

The $N=100$ transducers of each array were arranged[2] in a non-equidistant pattern, in order to be able to detect modes in the range $-80\le k\le 79$ $(K=160)$. For that purpose, the maximum absolute value of Π_k, Eq. (13), was minimized for $1\le k\le K-1$. The bypass array was optimized with the additional constraint of two non-accessible sectors[3]. The layout of both arrays and their PSFs (expressed in dB) are shown in Fig. 2 and Fig. 3. As can be seen in the PSF images, the optimisation process led to aliasing peaks at $k=160$. The dynamic range (level difference between Π_0 and $\max\{\Pi_k;\ k=1,\text{L},K-1\}$) is 19.56 dB for the bypass array and 22.64 dB for the intake array.

A measurement is considered here at 5515 RPM (60% engine speed). The measurement time was 10 s and the sample rate 44 kHz.

A breakdown of the average Sound Pressure Level (SPL) at both arrays into shaft tones and broadband noise is shown in Fig. 4. Only at the Blade Passing Frequency (BPF) and higher harmonics, i.e., where the shaft orders are multiples of the number of rotor blades (20), tones have significant levels. At other shaft orders broadband noise dominates.

3.1. Broadband noise

CB and NNLS were applied to broadband noise data at all shaft orders up to 100. First, the validity of the mode incoherence, as assumed in Section 2.3, was checked. This appeared to be the case, as illustrated for shaft order 75 in Fig. 5.

CB results are depicted in Fig. 6 and NNLS results in Fig. 7. Comparing CB with NNLS, we see virtually the same mode levels in the triangle of propagating modes. But outside the triangle, the NNLS levels are typically 10 dB lower[4]. At each shaft order, the NNLS results were summed and compared with

[2] Both arrays were designed within the EU 5th Framework project SILENCE(R) [23].
[3] The bypass array design process started with a non-constrained optimization which was compressed until the "forbidden" sectors were free of sensor locations. The final design was selected from a large number of trials.
[4] This also shows that aerodynamic pressure fluctuations, which do not have a preferred mode order, have much lower levels than the acoustic broadband noise.

the average SPL. A maximum difference of only 0.1 dB was found, thus demonstrating the high quality of the NNLS results.

3.2. Shaft tones

The MP method, outlined in Section 2.4, was applied to the BPF tones, i.e., to shaft orders 20, 40, 60, and 80. The iteration process was done with subsets of $K_{\text{sub}} = 30$ modes. For the 8 cases (intake and bypass) the number of iterations for obtaining the final subset of dominant modes varied between 4 and 9. The condition numbers of the matrix to be inverted, Eq. (30), remained below 10.

Results for, respectively, the bypass and the intake array are shown in Fig. 8 and Fig. 9. The images show a significant increase in dynamic range, featuring level reductions of 10 to 20 dB for modes that were apparently spurious, especially in the cut-off regime. For example, in the bypass results the rotor-stator interaction modes [4] ($k = \text{shaft order} \pm \nu \times 44$) show much more protrusion.

Interestingly, the rotor-stator interaction modes have also become prominent in the bypass array BPF results (shaft order = 20; mode orders = −68, −24, 20, 64), even though these modes are all cut-off. The reason for their presence is the short distance between the stator and the array. Note that a few aliased modes are visible too: $-112 + 160 = 48$ and $108 - 160 = -52$.

A check on the quality of the results can be made by comparing measured transducer pressures **p** with reconstructed pressures $\mathbf{Ga}_{\text{dec}}$. In Fig. 10 a comparison of the absolute values at shaft order 20 is shown, both for the intake and for the bypass array. The agreement is good.

4. Discussion

To assess the accuracy of the MP results discussed in the previous chapter, MP was also applied, with the same settings, to synthesized mode detection array data. The bypass array geometry (Fig. 2) was used. Array data were synthesized with two groups of modes:

- "Dominant modes": 15 mode orders were randomly selected between −30 and 30. Each mode was given a random SPL between −20 and 0 dB and a random phase.
- "Background modes": all the other modes were given a random phase too and a random SPL between −40 and −25 dB.

The CB and MP results are shown in Fig. 11. The improvement obtained with MP is obvious, especially for values between −20 and −10 dB.

It must be emphasized, however, that the success of MP depends on the actual distribution of modes. In particular, MP takes advantage of the "sparsity" of the dominant modes. That is, MP benefits from the fact the acoustic field is usually dominated by a limited set of modes. What happens when there is no sparse set of dominant modes is depicted in Fig. 12. Here array data were generated with "background modes" only, having random SPL between −5 and 0 dB and random phase. For this simulation, the CB results are poor, but the MP results are even worse.

Finally, for simulations with incoherent broadband noise modes it was found that the NNLS results always matched exactly (i.e., at machine precision) with the actual mode levels, regardless of the assumed mode distribution.

5. Conclusions

A deconvolution strategy is proposed for azimuthal mode detection with unequally spaced transducer rings. Different approaches for broadband noise and shaft-periodic tonal sound are followed. For broadband noise, a standard NNLS solver is recommended to solve the convolution equations, assuming the modes to be incoherent. For tones a MP algorithm is proposed, exploiting the fact that the acoustic field is usually dominated by a limited set of modes. The "best match" solution is found with an iterative search process, in which the total number of dominant modes is pre-defined.

The deconvolution strategy was applied to mode detection measurements in an AneCom fan rig. Compared to standard CB (here the same as DFT) results, an increase in dynamic range of typically 10 to 20 dB was found. The following quality checks were made:

a) For broadband noise the summed mode powers were compared with the average auto-powers. The agreement was within 0.1 dB.
b) For tones the mode amplitudes obtained with MP were used to reconstruct the transducer data, which were compared to the actual measurements. Excellent agreement was found.

The good performance of NNLS and MP was confirmed with synthesized data.

For fan rig measurements, the additional time needed for the deconvolution algorithms NNLS and MP is small compared to the computation time for CB, which is dominated by the averaging process needed to calculate $\mathbf{p}_{\text{ton}}$ and $\mathbf{C}_{\text{brb}}$.

Acknowledgments

The fan rig measurements were performed within the EU 6th Framework project PROBAND [24]. Assystem UK Ltd is acknowledged for providing the fan rig drawing of Fig. 1.

Appendix A: Incoherence of broadband noise modes in engine ducts

An acoustic field due to a point source in a circular duct can be expressed as a summation of modes:

$$p(\theta) = q\sum_k \lambda_k \exp\left[-\mathrm{i}\,k\left(\theta-\varphi\right)\right], \tag{A.1}$$

Herein, q is the source amplitude, λ_k are constants, and φ is the source angular position. In an engine duct, it can be expected that broadband noise sources are associated with blades in a blade row (e.g., a stator). Thus, groups of incoherent sources exist:

$$p(\theta) = \sum_{m=1}^{M} q_m \sum_k \lambda_k \exp\left[-\mathrm{i}\,k\left(\theta-\varphi_m\right)\right], \tag{A.2}$$

where M is the number of blades and φ_m their angular positions. Usually the blades are equally spaced, so we can write

$$\varphi_m = \frac{2\pi m}{M}. \tag{A.3}$$

Thus, mode amplitudes corresponding with Eq. (A.2) are

$$b_k = \lambda_k \sum_{m=1}^{M} q_m \exp\left[2\pi \mathrm{i} k \frac{m}{M} \right] \tag{A.4}$$

For the mode cross-powers we have

$$B_{kj} = \left\langle b_k b_j^* \right\rangle = \lambda_k \lambda_j^* \sum_{m=1}^{M} \sum_{n=1}^{M} \left\langle q_m q_n^* \right\rangle \exp\left[2\pi \mathrm{i} \frac{km - jn}{M} \right]. \tag{A.5}$$

Because the sources on different blades are incoherent, we obtain

$$B_{kj} = \left\langle b_k b_j^* \right\rangle = \lambda_k \lambda_j^* \sum_{m=1}^{M} \left\langle q_m q_m^* \right\rangle \exp\left[2\pi \mathrm{i} (k - j) \frac{m}{M} \right]. \tag{A.6}$$

The assumption that all sources have the same, unit, strength yields

$$B_{kj} = \lambda_k \lambda_j^* \sum_{m=1}^{M} \exp\left[2\pi \mathrm{i} (k - j) \frac{m}{M} \right]. \tag{A.7}$$

Eq. (A.7) is zero, unless $j = k + \nu M$ for integer values of ν. In other words, mode cross-powers in engine ducts are expected to be zero, unless the difference between the mode orders is a multiple of the number of blades.

Note that the analysis above ignores the presence of multiple, incoherent radial modes. This will probably reduce also the cross-powers when $j = k + \nu M$.

References

[1] E.R. Rademaker, P. Sijtsma, B.J. Tester, Mode detection with an optimised array in a model turbofan engine intake at varying shaft speeds, AIAA Paper 2001-2181, 2001.

[2] J. Lan, J. Premo, G. Zlavog, C. Breard, B. Callender, M. Martinez, Phased array measurements of full-scale engine inlet noise, AIAA Paper 2007-3434, 2007.

[3] S.L. Sarin, E.R. Rademaker, In-flight acoustic mode measurements in the turbofan engine inlet of Fokker 100 aircraft, AIAA Paper 93-4414, 1993.

[4] J.M. Tyler, T.G. Sofrin, Axial flow compressor noise studies, *SAE Transactions* 70 (1962), 309-332.

[5] A.G. Prinn, R. Sugimoto, R.J. Astley, The effect of steady flow distortion on noise propagation in turbofan intakes, AIAA Paper 2016-3028, 2016.

[6] P. Sijtsma, Using phased array beamforming to identify broadband noise sources in a turbofan engine, *International Journal of Aeroacoustics* 9 (3) (2010) 357-374.

[7] L. Enghardt, U. Tapken, W. Neise, F. Kennepohl, K. Heinig, Turbine blade/vane interaction noise: acoustic mode analysis using in-duct sensor rakes, AIAA Paper 2001-2153, 2001.
[8] U. Tapken, R. Bauers, L. Neuhaus, N. Humphreys, A. Wilson, C. Stöhr, M. Beutke, A new modular fan rig noise test and radial mode detection capability, AIAA Paper 2011-2897, 2011.
[9] L. Heidelberg, D. Hall, Inlet acoustic mode measurements using a continuously rotating rake, *AIAA Journal of Aircraft* 32 (1995) 761-767.
[10] P. Sijtsma, H. Orsi, Azimuthal and radial mode detection by a slowly rotating rake, AIAA Paper 2013-2244, 2013
[11] M. Behn, R. Kisler, U. Tapken, Efficient azimuthal mode analysis using compressed sensing, AIAA Paper 2016-3038, 2016.
[12] W. Yu, X. Huang, Compressive sensing duct mode detection method with in-duct microphone array, AIAA Paper 2016-2765, 2016
[13] R.P. Dougherty, Extensions of DAMAS and benefits and limitations of deconvolution in beamforming, AIAA Paper 2005-2961, 2005.
[14] T.F. Brooks, W.M. Humphreys, Jr., A deconvolution approach for the mapping of acoustic sources (DAMAS) determined from phased microphone array, *Journal of Sound and Vibration* 294 (4-5) (2006) 856-879.
[15] T.F. Brooks, W.M. Humphreys, Jr., Extension of DAMAS phased array processing for spatial coherence determination (DAMAS-C), AIAA Paper 2006-2654, 2006.
[16] P. Sijtsma, CLEAN based on spatial source coherence, *International Journal of Aeroacoustics* 6 (4) (2007) 357-374.
[17] T. Yardibi, J. Lia, P. Stoica, L.N. Cattafesta III, Sparsity constrained deconvolution approaches for acoustic source mapping, *Journal of the Acoustical Society of America* 123 (5) (2008) 2631-2642.
[18] R.P. Dougherty, G.G. Podboy, Improved phased array imaging of a model jet, AIAA Paper 2009-3186, 2009.
[19] T. Padois, A. Berry, Orthogonal matching pursuit applied to the deconvolution approach for the mapping of acoustic sources inverse problem, *Journal of the Acoustical Society of America*.138 (6) (2015) 3678-3685
[20] P. Sijtsma, Acoustic beamforming for the ranking of aircraft noise, National Aerospace Laboratory NLR Report: NLR-TP-2012-137 (2012).
[21] J.A. Högbom, Aperture synthesis with a non-regular distribution of interferometer baselines, *Astronomy and Astrophysics* (Supplement Series) 15 (1974) 417-426.
[22] C.L. Lawson, R.J. Hanson, *Solving Least Squares Problems* (Chapter 23), SIAM, 1995.
[23] Summary of EU 5th Framework project SILENCE(R): "Significantly lower community exposure to aircraft noise", https://www.xnoise.eu/index.php?id=85, 2007 (accessed 6 February 2018).
[24] Summary of EU 6th Framework project PROBAND: "Improvement of Fan Broadband Noise Prediction: Experimental investigation and computational modelling", https://www.xnoise.eu/about-x-noise/projects/generation-2-projects/proband/, 2008 (accessed 6 February 2018).

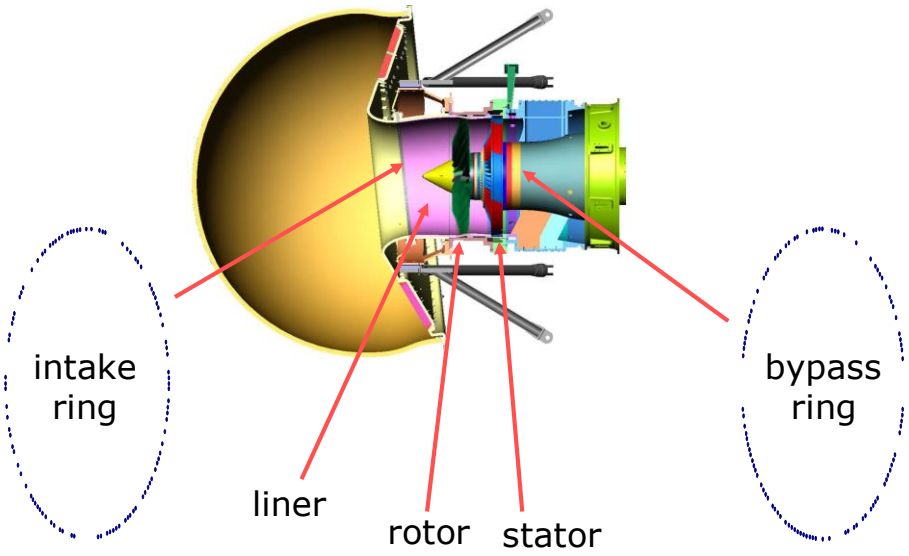

Fig. 1. Drawing of RR fan rig in AneCom AeroTest facility.

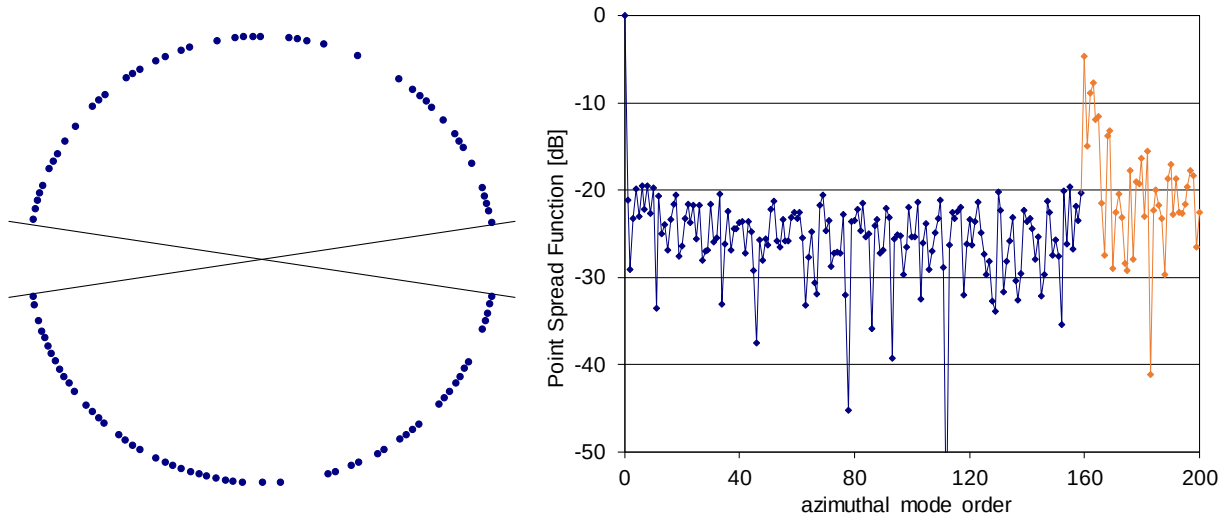

(a) (b)

Fig. 2. Layout of bypass array (a) and corresponding PSF (b)

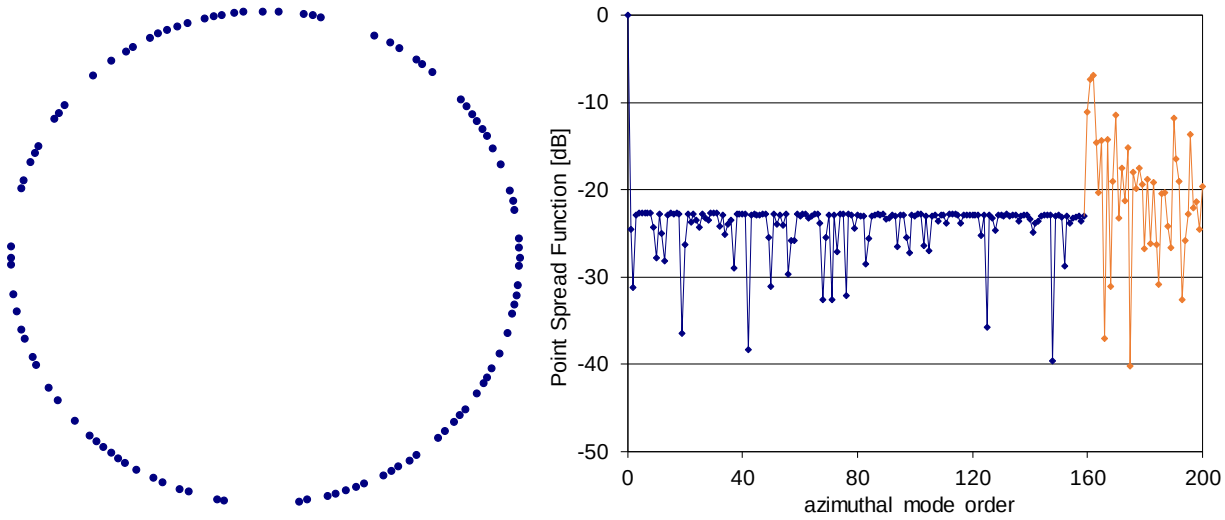

(a) (b)

Fig. 3. Layout of intake array (a) and corresponding PSF (b)

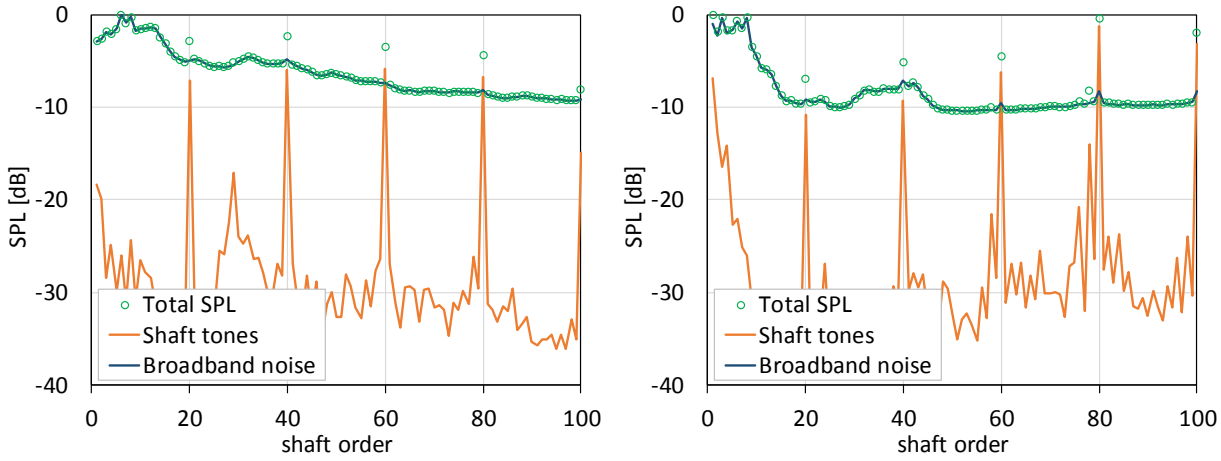

(a) (b)

Fig. 4. Average SPL; breakdown into shaft tones and broadband noise; bypass array (a) and intake array (b)

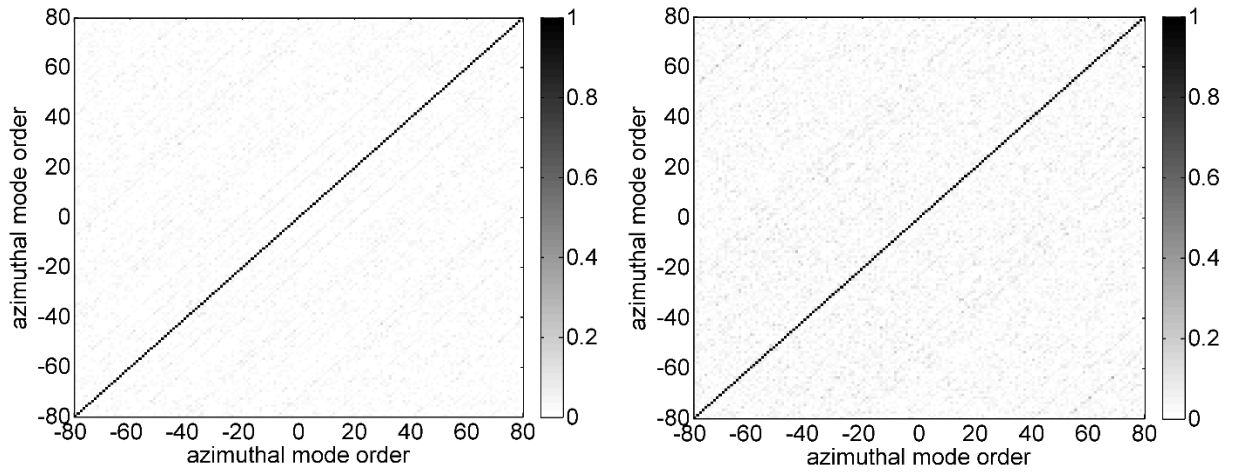

(a) (b)

Fig. 5. Broadband noise mode coherence at shaft order 75; bypass array (a) and intake array (b)

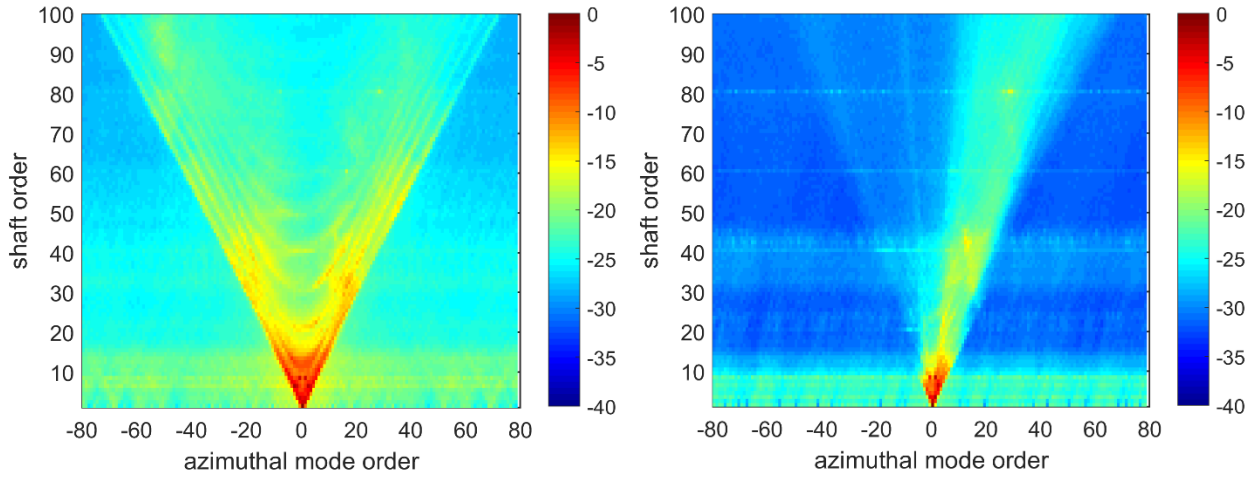

(a) (b)

Fig. 6. Broadband noise CB results; bypass array (a) and intake array (b)

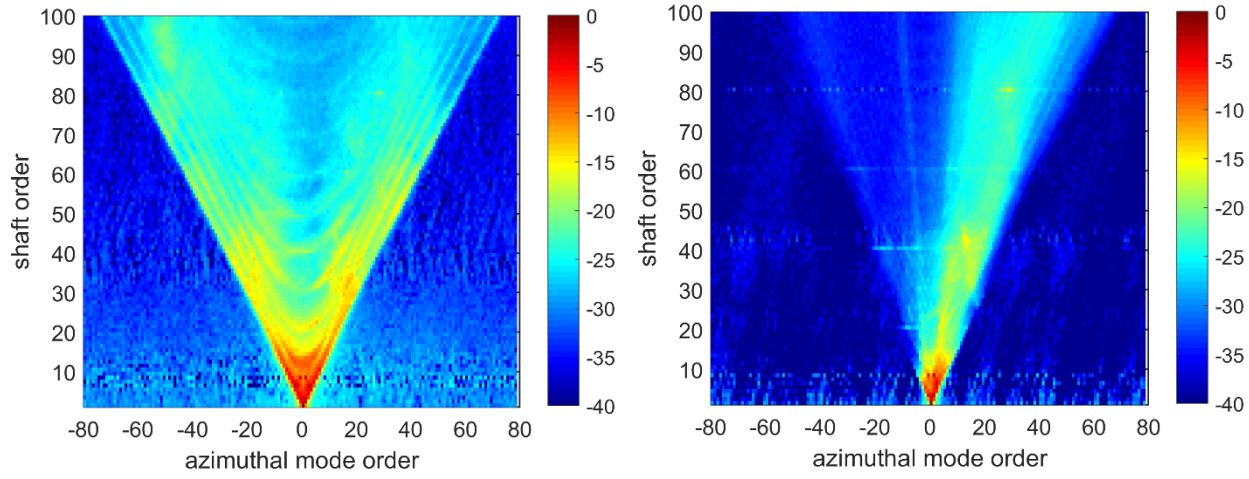

(a) (b)

Fig. 7. Broadband noise NNLS results; bypass array (a) and intake array (b)

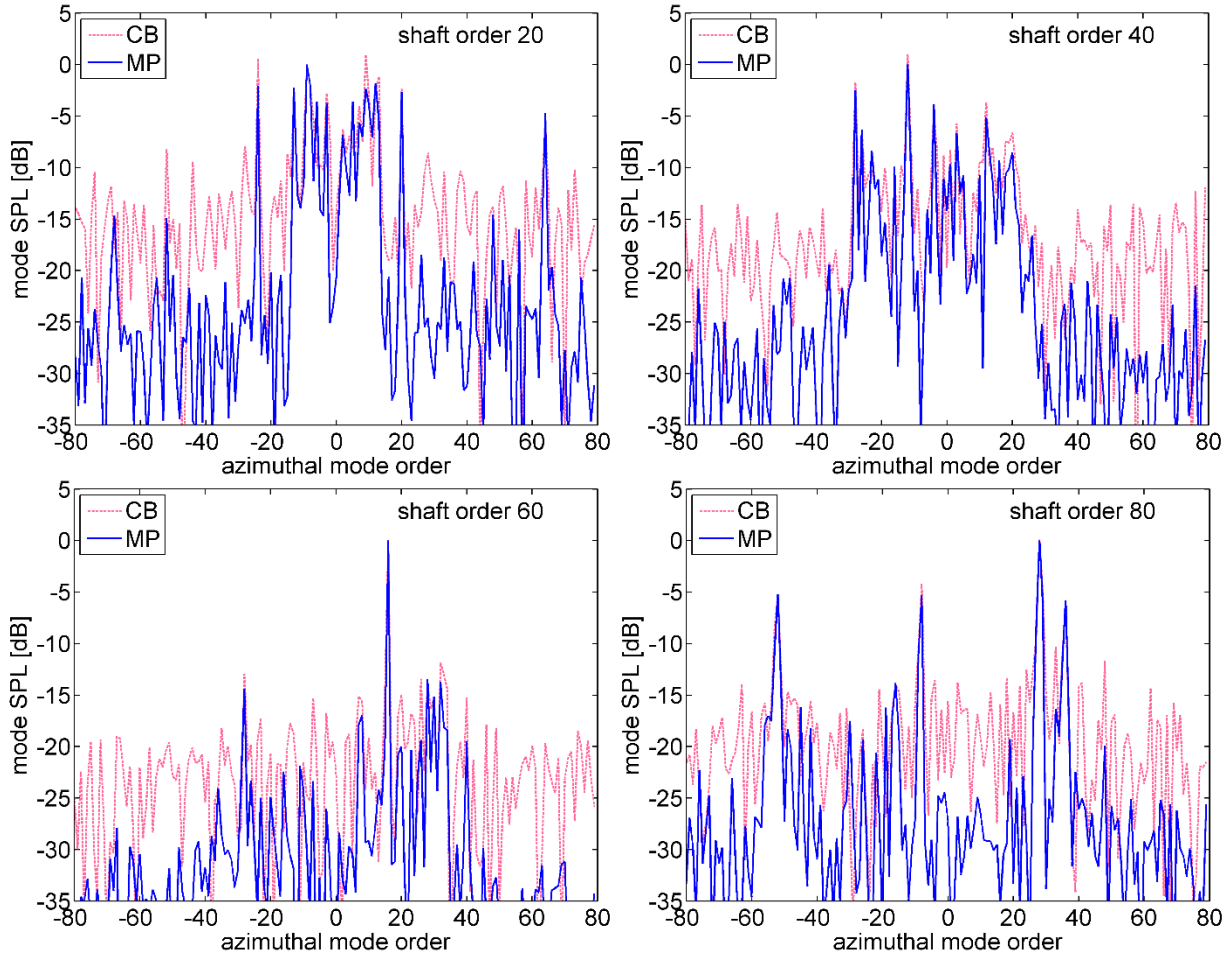

Fig. 8. CB and MP results for BPF tones; bypass array

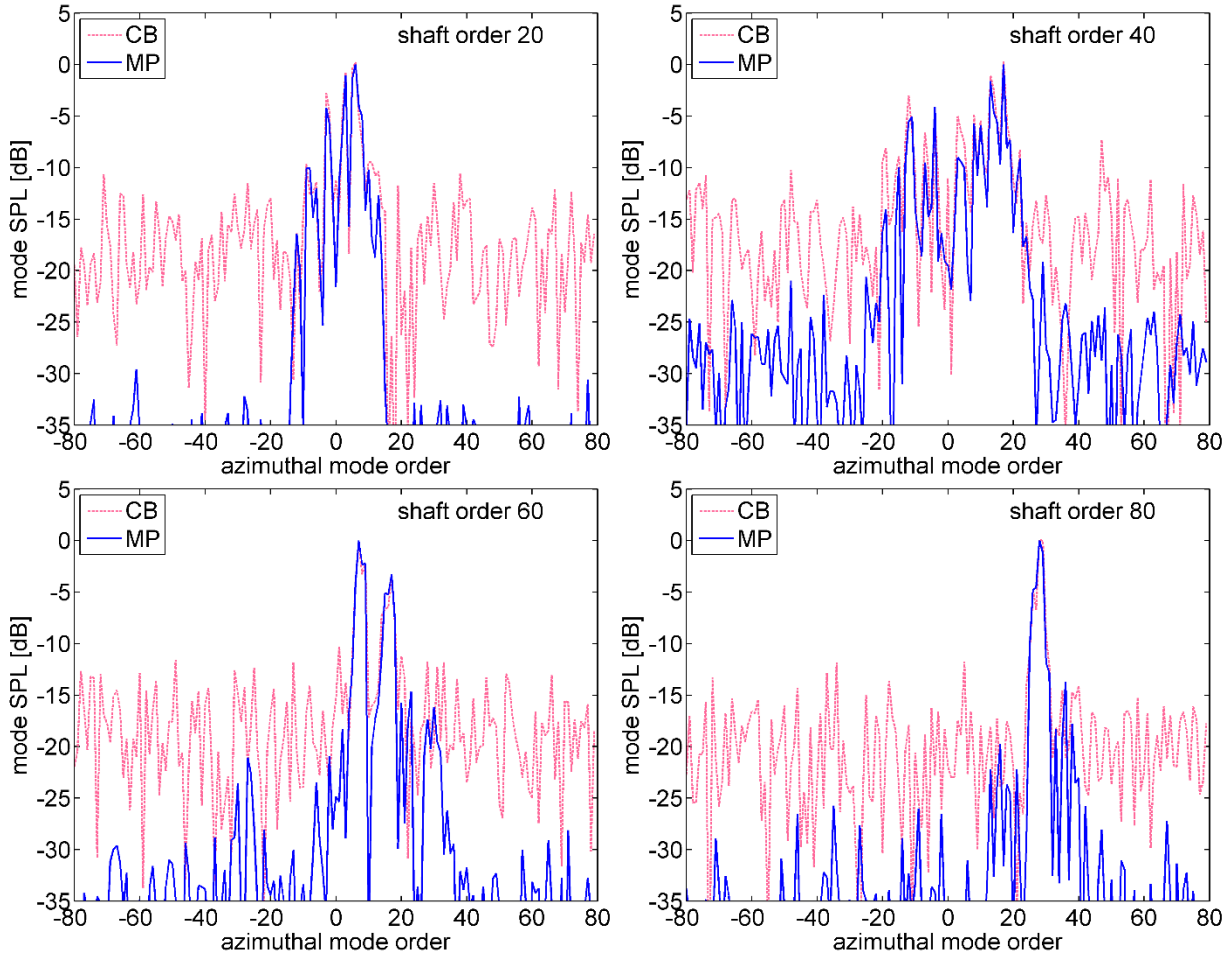

Fig. 9. CB and MP results for BPF tones; intake array

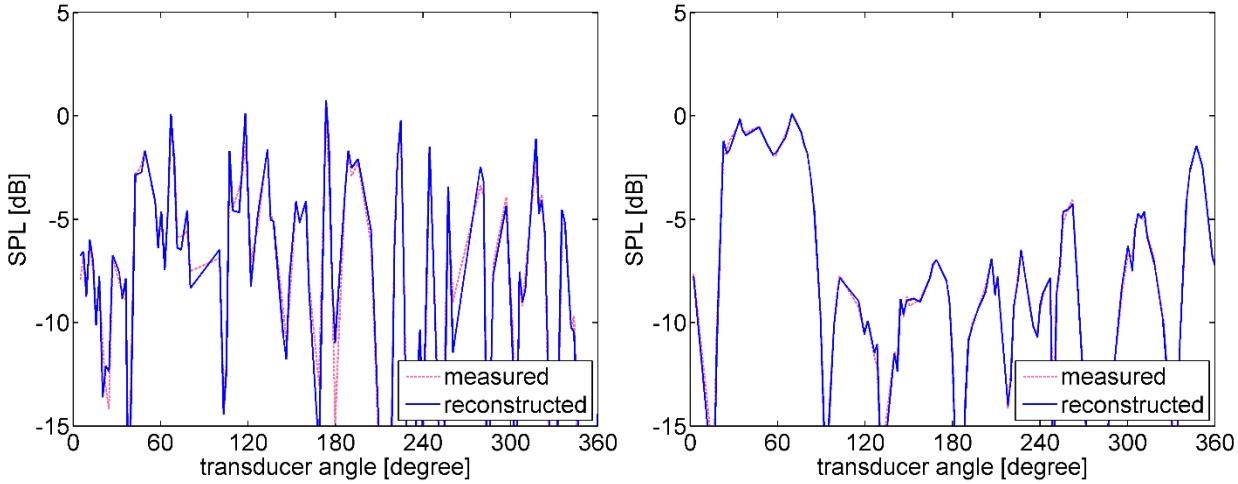

(a) (b)

Fig. 10. Measured and reconstructed transducer pressures at shaft order 20, absolute values; bypass array (a) and intake array (b)

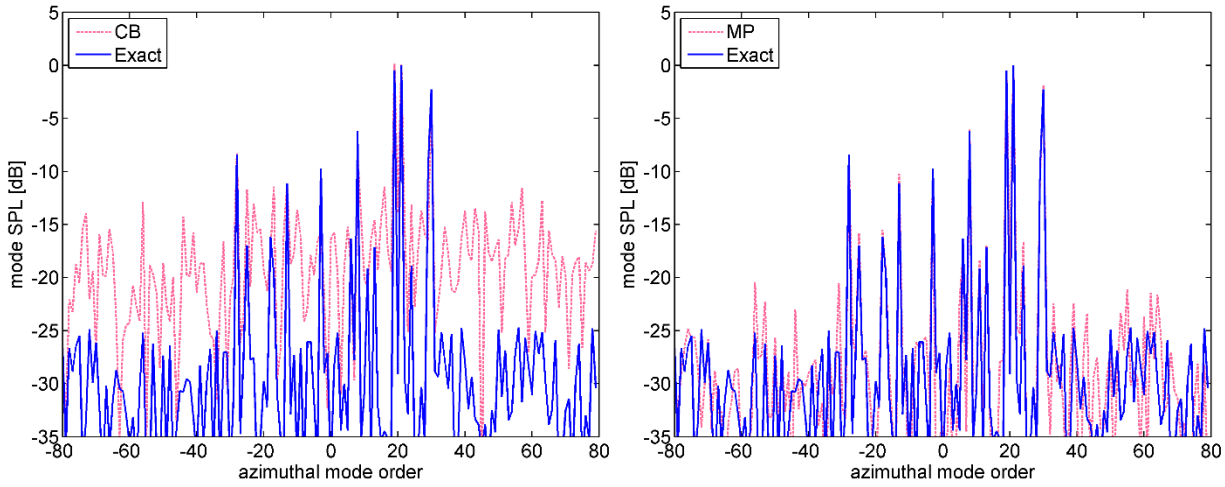

(a) (b)

Fig. 11. CB (a) and MP (b) results applied to synthesized data with a sparse set of dominant modes; bypass array

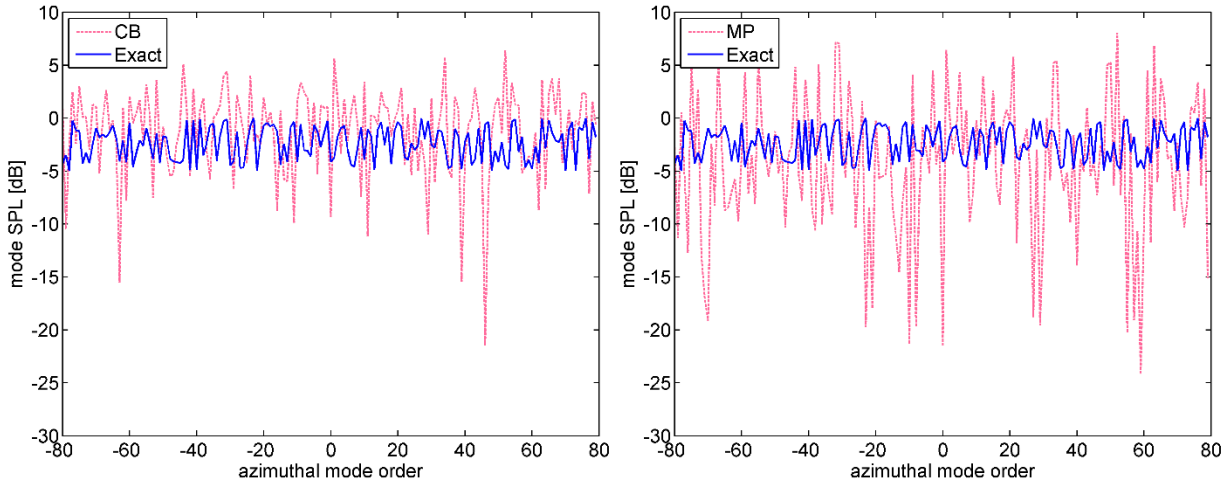

(a) (b)

Fig. 12. CB (a) and MP (b) results applied to synthesized data without a sparse set of dominant modes; bypass array